Toward ferroelectric AlN/GaN heterostructures and sputtered III-N thin films with metal organic chemical vapor deposition-like texture

Check for updates

Georg Schönweger [1,2] ✉, Niklas Wolff[1,3], Md Redwanul Islam[1], Isabel Streicher [4,5], Stefano Leone [4], Lorenz Kienle[1,3] & Simon Fichtner [1,2,3]

Merging III-N-technology and wurtzite ferroelectricity could enable novel devices with enhanced functionality, for instance, harsh environment ferroelectric non-volatile memories and neuromorphic components. However, no scalable fabrication approach to achieve this fusion is available to date, as wurtzite ferroelectrics such as $Al_{1-x}Sc_xN$ are hard to synthesize by metal organic chemical vapor deposition (MOCVD), the standard growth method for commercial III-N-devices. Sputtering as another high-throughput method does so far not reach the material quality that is necessary for III-N-technology. In this contribution, exceptional structural quality of $Al_{1-x}Sc_xN$ grown by sputter epitaxy onto GaN is demonstrated, featuring an out-of-plane mosaicity of just 258 arcsec - comparable to state of the art MOCVD and molecular beam epitaxy (MBE) processes. Furthermore, ferroelectric switching is observed in typically non-ferroelectric binary AlN grown by both sputtering and MOCVD onto GaN. Thus, two promising approaches to realize ferroelectric III-N heterostructures with high-throughput methods exist: lattice-matched sputtering of $Al_{1-x}Sc_xN$ on GaN and MOCVD-growth of binary AlN on GaN.

The wurtzite ferroelectrics are attractive functional materials for next-generation microelectronic devices. This CMOS-compatible, scalable, and inherently harsh environment resistant emerging material class has the potential to foster the development of non-volatile memory and memristive devices, as well as enhanced mechanical and optical devices, e.g., for efficient second harmonic generation[1–6]. Besides $Zn_{1-x}Mg_xO$, all of the wurtzite ferroelectrics demonstrated experimentally are III-N-based compounds and thus naturally compatible with III-N-technology. In particular, the recent demonstration of ferroelectric $Al_{1-x}Sc_xN$ grown by metal organic chemical vapor deposition (MOCVD - the most common commercial growth method of epitaxial III-N thin films) could advance the integration of ferroelectric functionality in III-N devices such as reconfigurable normally-off high electron mobility transistors (HEMT)[7]. However, the establishment of a high-throughput $Al_{1-x}Sc_xN$ MOCVD growth process remains challenging due to the low vapor pressure of the Sc precursor, and crucial aspects like scalability to the sub-20-nm thickness range remain unresolved[7–9]. The availability of binary Sc-free III-N ferroelectrics would

simplify, in particular, the MOCVD process and, in general, lower the production costs as well as the environmental impact, thus advancing the development of ferroelectric III-N-based devices.

The electric field-driven inversion of the spontaneous polarization in the wurtzite structure is only achievable if the coercive field (E_c) is lower than the breakdown field (E_b). However, the E_c/E_b ratio in III-N-based ferro-electrics is not only determined by the stoichiometry of the typically ternary compound, but also depends on the stress or strain state, the interfaces, and the environment. For binary AlN, it was demonstrated that when switching at higher temperatures or if grown epitaxially on semiconducting $SrTiO_3$ templates, E_c decreases below E_b, and also the binary compound has to be considered as ferroelectric[10,11]. Furthermore, the concept of proximity ferroelectricity was suggested recently, enabling the propagation of polar domains across interfaces into typically non-ferroelectric wurtzite-type materials (e.g., AlN) by stacking it with a layer of a wurtzite ferroelectric (e.g., $Al_{1-x}Sc_xN$)[12]. However, ferroelectricity in binary AlN/III-N heterostructures is yet unexplored.

[1]Department of Material Science, Kiel University, Kiel, Germany. [2]Fraunhofer Institute for Silicon Technology (ISIT), Itzehoe, Germany. [3]Kiel Nano, Surface and Interface Science (KiNSIS), Kiel University, Kiel, Germany. [4]Fraunhofer Institute for Applied Solid State Physics (IAF), Freiburg, Germany. [5]Consiglio Nazionale delle Ricerche - Istituto per la Microelettronica e Microsistemi (CNR-IMM), Catania, Italy. ✉e-mail: gmsc@tf.uni-kiel.de

On the other hand, wurtzite ferroelectrics grown by the established high-throughput sputter-deposition method typically lack the high structural quality of MOCVD- and molecular beam epitaxy (MBE)-grown films. For introducing ferroelectric functionality into III-N devices, reaching this structural quality is not obligatory as long as the ferroelectric layer is separated from the active heterojunction by a barrier layer. This was demonstrated for $Al_{1-x}Sc_xN$ sputter-deposited onto the gate stack of a high electron mobility transistor (FeHEMT)[13]. However, the active heterojunctions of III-N devices require high structural and interfacial quality for proper device functionality and performance. Matching these requirements through sputter epitaxy would enable low-cost, high-throughput production of such heterojunctions at a much lower thermal budget during deposition (typically well below 500 °C) compared to MOCVD. The latter would prevent atomic interdiffusion, which is commonly observed for MOCVD-grown heterostructures[8]. Furthermore, sputter epitaxy of III-N thin films with MOCVD-like structural quality would open prospects for all-epitaxial device concepts and functionalities, as well as it would simplify the design of ferroelectric III-N devices. In a FeHEMT, for instance, the ferroelectric barrier layer could not only induce the transistor's channel (i.e., the two-dimensional electron gas - 2DEG), but also intrinsically modulate this channel through ferroelectric switching[14].

One characteristic reflecting the structural quality is the out-of-plane mosaicity, which for wurtzite-type materials can be quantified by the rocking curve full width at half maximum (RC-FWHM) of the 0002 reflection. The latter was reported to be as low as 106 arcsec for MBE-grown ($x = 0.14$)[15] and 257 arcsec for MOCVD-grown ($x = 0.15$)[8] $Al_{1-x}Sc_xN$ on GaN/Sapphire templates, respectively. Recently, an out-of-plane mosaicity of 692 arcsec was reported for sputter-deposited $Al_{1-x}Sc_xN$ ($x = 0.10$)[16] coherently grown on a bulk GaN substrate. This indicates that the mosaicity of MBE- and MOCVD-grown films is potentially reachable also by lattice-matched sputter epitaxy of III-N heterostructures.

In this study, the ferroelectric response and structure of $Al_{1-x}Sc_xN$ and AlN grown by sputter epitaxy (x ranging from 0 to 0.28) as well as by MOCVD (AlN) on n-type (Si) doped GaN/Sapphire templates is investigated. Ferroelectricity in unsubstituted AlN/GaN is unveiled, which includes 100-nm-thin crack-free sputter-deposited as well as 5-nm-thin pseudomorphic MOCVD-grown AlN. Thus, the availability of ferroelectric AlN for III-N-technology grown by a high-throughput MOCVD process is demonstrated. Additionally, ferroelectric switching in 5-nm-thin AlN at ≈2 V highlights the scaling potential and suitability for low-voltage and low-power operation of future all-III-N ferroelectric devices. Furthermore, an exceptional structural quality of $Al_{1-x}Sc_xN$ (out-of-plane mosaicity of 258 arcsec) grown on GaN by sputter epitaxy approaching the mosaicity of the underlying GaN template at close to lattice-matched conditions ($x = 0.08$ and $x = 0.11$) is revealed - a significant progress toward functional sputter-deposited III-N heterostructures.

The following discussion starts with X-ray diffraction analysis (XRD), revealing the structure and epitaxial characteristics of $Al_{1-x}Sc_xN$(100 nm,

$0 < x < 0.28$) and AlN grown by sputter epitaxy on GaN. This is followed by an in-depth study of transient current measurements revealing the ferroelectric characteristics in dependence on x, which are related to the structural properties. Furthermore, the ferroelectric response of AlN(5 nm)/GaN grown by MOCVD is investigated and compared. In the last section, advanced scanning transmission electron microscopy (STEM) and energy-dispersive X-ray spectroscopy (STEM-EDS) investigations are presented, revealing the interface properties in the MOCVD-grown AlN/GaN heterostructure as well as the manifestation of epitaxial strain and the polarization inversion on the atomic scale of pure AlN.

Results and discussion
Structural properties
The addition of Sc to AlN not only induces ferroelectricity, but also allows for systematic adjustment of the in-plane lattice parameter of $Al_{1-x}Sc_xN$ to match that of GaN. This ability to achieve lattice-matched growth conditions promises a reduced density of structural defects such as dislocations, without compromising on layer thickness[17,18]. However, deviations from these conditions introduce epitaxial strain, which strongly affects the ferroelectric properties[19]. In the following, the correlation between epitaxial strain, the ferroelectric properties, and the structural quality is examined for $Al_{1-x}Sc_xN$(100 nm)/GaN heterostructures and compared to unsubstituted AlN/GaN, changing the epitaxial growth conditions by variation of the Sc content ($0 < x < 0.28$) using sputter-deposition. First, the resulting layer quality is discussed in terms of the mosaicity, the lattice parameters, as well as reciprocal space maps in dependence on x.

The lattice parameters were extracted from $\theta - 2\theta$ and $2\theta - \omega$ XRD scans by evaluating the $Al_{1-x}Sc_xN$ 0002 and $10\bar{1}5$ reflections. Figure 1a depicts the a- and c-lattice parameters in dependence on Sc content. The Sc content was determined via scanning electron microscope energy-dispersive X-ray spectroscopy (SEM-EDS), for which we estimate an error of ±2 at.%.

Overall and congruent to calculations and experiments on relaxed $Al_{1-x}Sc_xN$[20,21], the a- and the c-lattice parameters are decreasing with decreasing Sc content. However, in the case of $Al_{1-x}Sc_xN$/GaN heteroepitaxy, the lattice parameters are in addition affected by epitaxial strain and film thickness. Depending on the Sc content and the associated in-plane lattice-mismatch, an epitaxially strained interface volume and gradual strain relaxation across a specific critical thickness is expected[19]. Hence, the lattice parameters determined via XRD always reflect the averaged values, including relaxed and strained volumes. The impact of epitaxial strain is in particular visible for $0.08 < x < 0.18$, revealing a-lattice parameters which are close to the measured a-lattice parameter of the GaN template (dashed line). The pseudomorphic epitaxial growth complicates the determination of the exact relaxed lattice-matched composition, especially for thinner films. At $x = 0.18$, compressive strain is reflected by the comparably small a- and large c-lattice parameter, deviating from the reported almost linear trend. Reducing x to 0.11 results in a jump in c-lattice parameter to lower values, while the a-lattice parameter is still congruent to the one of GaN when

Fig. 1 | Lattice parameters and texture of sputtered $Al_{1-x}Sc_xN$ on GaN. a Lattice parameters a and c of 100-nm-thin $Al_{1-x}Sc_xN$ grown by sputter epitaxy on GaN templates in dependence of Sc content. The black dashed lines correspond to the relaxed a-lattice parameter of AlN and the measured a-lattice parameter of the GaN template. **b** Corresponding FWHM of the $Al_{1-x}Sc_xN$ 0002 RC in dependence on the Sc content. The values for ferroelectric MOCVD[7] and MBE[4]-grown $Al_{1-x}Sc_xN$/GaN heterostructures, as well as the FWHM of the 0002 RC of the GaN template (dashed line), are included for comparison.
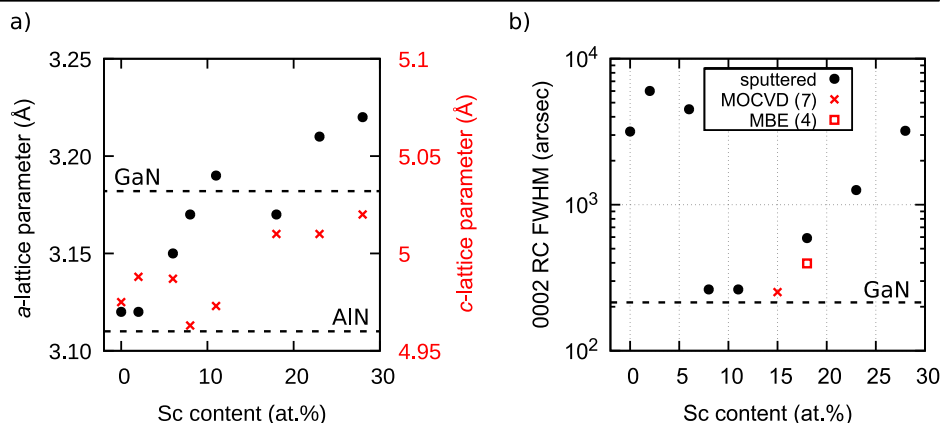
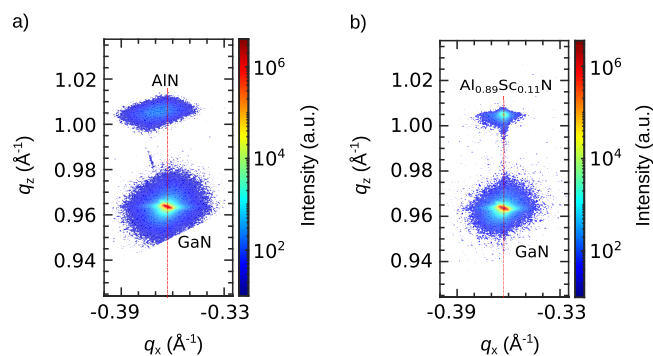**Fig. 2 | High-resolution reciprocal space maps.** RSM of the $10\bar{1}5$ reflections of sputtered 100-nm-thin **a** AlN and **b** $Al_{0.89}Sc_{0.11}N$ grown on GaN.

considering an error margin of 1 pm. This jump indicates a more relaxed or even tensilely strained lattice for $x = 0.11$. Thus, based on this measurement, lattice-matching is expected close to $x = 0.11$.

Figure 1b depicts the out-of-plane mosaicity, i.e., the tilt of the c-axis with respect to the surface normal, in dependence on the Sc content. For $x = 0.08$ and $x = 0.11$, the FWHM of the $Al_{1-x}Sc_xN$ 0002 rocking curve is lowest and amounts to only 258 arcsec and 261 arcsec, indicating close to lattice-matched growth to the GaN. Crucially, at these concentrations, the measured out-of-plane mosaicity approaches the benchmark of the GaN template (214 arcsec) and is comparable to what is reported for ferroelectric single-crystal-like $Al_{1-x}Sc_xN$ films grown by MOCVD (252 arcsec) and by MBE (≈400 arcsec)[4,7]. The in-plane mosaicity (i.e., the spread of the a-axis tilt within the plane of the layer) of the lattice-matched sputtered $Al_{1-x}Sc_xN$ layers approaches the in-plane mosaicity of the GaN template as well, which is reflected by the FWHM of the $Al_{1-x}Sc_xN$ $10\bar{1}2$ phi scan for $x = 0.08$, $x = 0.11$, and GaN, amounting to 990 arcsec, 864 arcsec, and 778 arcsec, respectively. A comparison of the $10\bar{1}2$ phi scan of GaN and $Al_{0.92}Sc_{0.08}N$ is given in Supplementary Fig. 1. This highlights the excellent crystal quality obtainable through sputter epitaxy when providing a lattice-matched template. This finding can be considered an important step toward a broader applicability of sputtered III-N thin films integrated into GaN-based heterostructures.

Additionally, while early density functional theory (DFT) calculations predicted lattice-matching of $Al_{1-x}Sc_xN$/GaN at $x = 0.18$[22], our results align with more recent experimental studies on MBE-grown and sputtered films demonstrating lattice-matched growth for $0.09 < x < 0.14$[15–18]. However, lattice-matching likely depends on the growth method and conditions, such as temperature and thermal expansion coefficient match between the individual layers and the substrate, and its precise determination is further complicated due to expected errors in the determination of the exact Sc content.

To further analyze the epitaxial growth, reciprocal space maps (RSM) of AlN and $Al_{0.89}Sc_{0.11}N$ were recorded and are depicted in Fig. 2.

The broad $10\bar{1}5$ reflection of the AlN spanning over the q_x center of the $10\bar{1}5$ GaN reflection suggests the presence of in-plane epitaxial tensile strain in AlN grown on GaN. The extension toward lower q_x values of the AlN $10\bar{1}5$ reflection is indicative of strain relaxation. In comparison, the $10\bar{1}5$ $Al_{0.89}Sc_{0.11}N$ reflection is much sharper, and its q_x position of highest intensity matches the q_x center of the $10\bar{1}5$ GaN reflection, although the asymmetry extending toward lower q_x values indicates the presence of slight tensile strain.

Ferroelectric properties

In this section, transient current measurements are discussed, revealing the ferroelectric characteristics of $Al_{1-x}Sc_xN$ ($0 < x < 0.28$) and AlN grown on GaN. The x-dependent electrical response is discussed by considering the dependence of epitaxial strain on x, as revealed in the "Structural properties" section. It is shown that epitaxy on GaN enables saturated polarization switching for all investigated Sc concentrations, including unsubstituted

AlN. This holds not only true for sputter-deposited 100-nm-thin AlN, but also for 5-nm-thin pseudomorphic AlN/GaN grown by MOCVD.

Figure 3a depicts the current density in dependence on the electric field (J–E loops) of the 100-nm-thin $Al_{1-x}Sc_xN$ sputter-deposited on GaN (see also Supplementary Fig. 2).

Distinct ferroelectric displacement current peaks are evidenced in all $Al_{1-x}Sc_xN$/GaN heterostructures as well as in the AlN/GaN. In comparison to non-switching AlN grown on Si, the ability of ferroelectric switching in AlN/GaN heterostructures is supported via forcing an in-plane tensile strain onto the AlN basal plane by interfacing with GaN, corresponding to a tensile strain of 2.5%, see Fig. 5f[23]. The delayed relaxation of this epitaxial lattice strain can shift the onset of the switching field to smaller electric fields below the breakdown field[24]. Thus, we demonstrate experimentally that also solely the deformation of the wurtzite lattice by epitaxial strain, next to local chemical disturbance by Sc addition, can enable ferroelectric switching in typically non-ferroelectric wurtzite-type materials. Similar to ferroelectric experiments on layered structures[12,25], more tensile-strained volumes preferentially facilitate the nucleation of domains with opposite polarization direction, which can then extend through the remaining volume.

The peak shape of the ferroelectric displacement current reflects the switching dynamics, which involve the formation of inversion domain nuclei and domain growth[7,26–29]. In general, the broader the peak, the more gradual the switching process. Referring to the positive branch of the J–E loops shown in Fig. 3a, the peak is the narrowest for the lattice-matched conditions ($x = 0.08$ and 0.11). The associated abrupt switching is potentially correlated to the narrow out-of-plane mosaicity of these films (cf. Fig. 1b). At the negative branch, a broadening of the switching regime and the emergence of two displacement current peaks are evident when passing $x > 0.02$. In our prior work, we related this peculiarity to depletion of the GaN as well as to epitaxially strained and relaxed volume fractions, which switch their polarization at different electric fields[19]. On the other hand, in films with $x \leq 0.06$, we observe that the hysteretic area of the negative branch gets smaller with decreasing Sc content, and the double peak disappears. Both phenomena can indicate that in spite of the saturated J–E curves, significant pinned volume remains for lower Sc concentrations, in particular for $x \leq 0.02$.

Figure 3b depicts the remanent polarization (P_r) in dependence on the Sc content, which was corrected for static leakage by performing positive up negative down (PUND) measurements. The P_r shows only slight variations in the range of $0.08 < x < 0.28$, with an average of ≈150 μC/cm². For non-epitaxial relaxed $Al_{1-x}Sc_xN$, P_r can be expected to increase with decreasing x[20,21]. For $Al_{1-x}Sc_xN$/GaN heterostructures with Sc contents in the range of $0.11 < x < 0.28$, compressive epitaxial strain counteracts, at least partially, the in-plane lattice expansion due to Sc incorporation, which can explain the almost constant P_r. However, for $x < 0.06$, the apparent P_r decreases with decreasing x when switching from nitrogen (N)-polarity to metal (M)-polarity and increases when switching vice versa. The measured drop in P_r is consistent with the disappearance of the second switching peak (Peak B_{neg}) for $x \leq 0.02$ and further supports partial ferroelectric switching from N- to M-polarity reflected in the negative branch of the J–E loop. The increase of P_r for these concentrations when switching from M- to N-polarity (positive branch) can be explained by dynamic leakage contributions, which we relate to the emergence of domain walls with enhanced conductivity during ferroelectric switching and thus can not be compensated by PUND[6,30]. In the extreme case of AlN, this results in a physically unrealistic P_r value above 300 μC/cm², as depicted in Supplementary Fig. 3. Nevertheless, the saturated J–E loop and the measured P_r of ≈75 μC/cm² at the negative branch indicate that a considerable part of the AlN thin film switched. Furthermore, increasing the epitaxial coherence of the GaN by, e.g., decreasing the AlN film thickness is expected to facilitate polarization reversal of the full volume.

The as-grown polarity of all films was investigated by applying unipolar voltage signals to pristine capacitors, as depicted in Supplementary Fig. 4. For $x = 0$ and $x = 0.08$, the switching polarization revealed that its associated volume was deposited as M-polar, see Supplementary Fig. 4a, d. For all other

Fig. 3 | Ferroelectric properties of sputtered $Al_{1-x}Sc_xN$ and AlN on GaN. a J–E loops in dependence of Sc content measured at 40 kHz. Prior to the actual measurement, each sample was cycled 200 times to reduce differences in imprint. **b** The PUND corrected apparent switching polarization $2P_r$ in dependence on the Sc content determined at 40 kHz using a triangular voltage signal. Switching at the positive branch in (**a**) corresponds to the M-to-N-polarity inversion, and switching at the negative branch corresponds to the N-to-M-polarity inversion. The error bars are calculated via error propagation by assuming an error of 1 μm in the capacitors' diameter due to limited lithography capabilities. **c** The electric field extracted from (**a**) at which the displacement current locally peaks in dependence on the Sc content. For 0 and 8 at.% Sc, the exact film thickness was determined by TEM, while for all other Sc contents, error bars are included by assuming an error in film thickness of 5 nm.
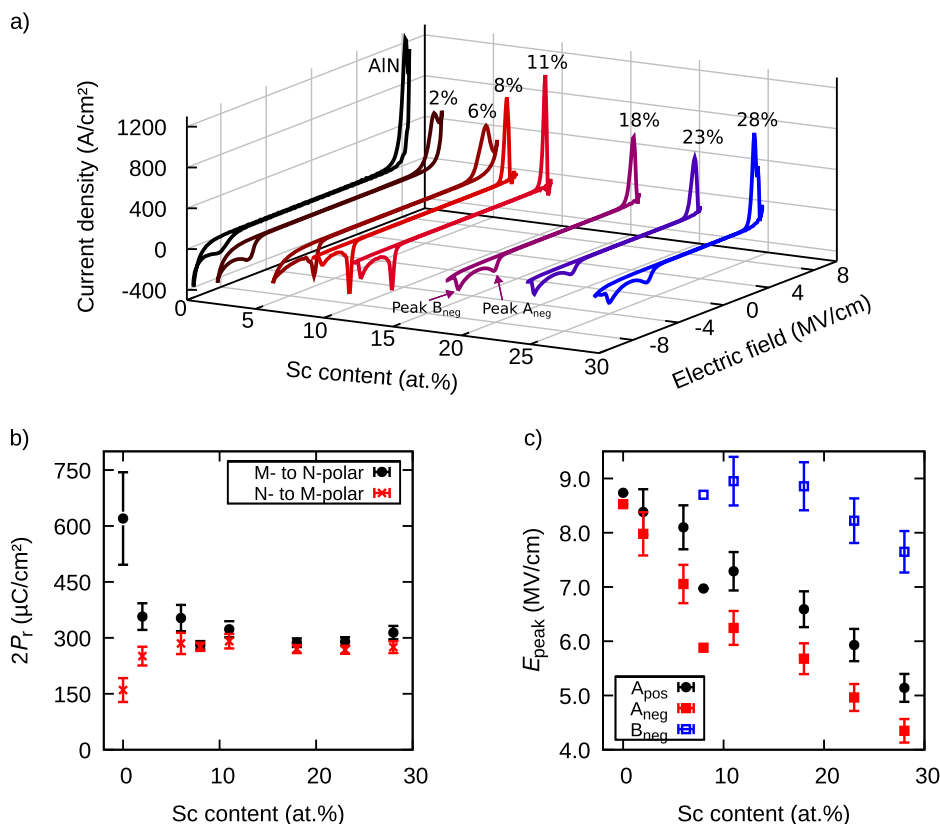
films, mixed polarity is present after growth. In the past, we could demonstrate the existence of a presumably horizontal antiphase (i.e., as-grown inversion) boundary in as-grown $Al_{0.72}Sc_{0.28}N$/GaN heterostructures, at which the interfacial M-polar domain inverts into an N-polar domain at around 30–40 nm above the interface to the GaN[19]. The natural emergence of this antiphase boundary was suggested to be interrelated with the observed epitaxial strain relaxation from the compressively strained volume near the GaN interface. Likewise, strain relaxation also takes place for the tensile-strained films with $x \leq 0.02$, as supported by our TEM investigations ("Atomic-scale investigations" section). Assuming an N-polar relaxed volume fraction in the upper part of AlN, this volume would be non-switchable due to the absence of electrically determined as-grown N-polarity. This can also serve to explain the decrease of $2P_r$ to 150 μC/cm². On the other hand, no indication of a mixed polar nature of the sample with $x = 0.08$ emerged, which is an additional indication of high structural quality and coherence.

Similar to P_r, lattice deformation and epitaxial strain affect the coercive field, i.e., tensile strain results in a decrease and compressive strain results in an increase of E_c[23,31,32]. Figure 3c depicts the electric field at which the displacement current locally peaks in dependence on the Sc content. In contrast to the negative branch, the ferroelectric displacement current at the positive branch (A_{pos}) is not affected by depletion and peak splitting and is therefore appropriate for deriving E_c. E_c as well as E_{peak} of A_{neg} and B_{neg} increase nearly linearly with decreasing Sc content, showing slight deviations only for $x = 0.08$. A linearly decreasing trend is also reported for relaxed $Al_{1-x}Sc_xN$ grown non-epitaxially on Pt[20]. The observed drop in E_{peak} suggests the presence of significant epitaxial tensile strain for $x = 0.08$, which also implies that for lattice-matching, x has to be larger, consistent with the data presented in the "Structural properties" section.

Motivated by these results, we investigated ferroelectricity in AlN/GaN heterostructures grown by a standard high-throughput MOCVD growth process. The critical film thickness of MOCVD-grown AlN on GaN

amounts to ≈5 nm, after which structural degradation and cracking are observed[33,34]. This is in strong contrast to the remarkable strain relaxation capabilities of sputtered AlN (see "Atomic-scale investigations" section), which prevents the formation of cracks even for 100-nm-thick films. On the other hand, in the case of MOCVD-grown AlN (5 nm)/GaN heterostructures, the reported full pseudomorphic growth, i.e., the whole volume is fully tensile-strained to the GaN template[35], is expected to result in facilitated ferroelectric switching capabilities. However, as a consequence of the relatively high temperatures applied during MOCVD growth, AlN deposition actually results in a chemically graded Al(Ga)N layer due to interfacial atomic diffusion at these small length scales, see "Atomic-scale investigations" section[34,36]. The electric characterization of this 5-nm-thin Al(Ga)N layer depicted in Fig. 4 shows clear ferroelectric behavior in direct comparison to the ferroelectric response of the sputter-deposited 100-nm-thin AlN.

At the positive branch, the 5-nm-thin film exhibits a displacement current peak comparable to other wurtzite ferroelectrics, while for the negative branch, a broad hysteresis area emerges due to the semi-conducting substrate. Non-switching cycles are included in red and allow for distinguishing between ferroelectric displacement and leakage currents. At the negative branch of the loop, the applied voltage not only drops across the Al(Ga)N layer but also across the depleted GaN[19], which explains the high apparent electric field required to switch the 5-nm-thin film from N- to M-polarity. Frequency-dependent measurements (Supplementary Fig. 5) reveal an increase of E_c and an increase of the displacement currents with increasing frequency, as expected for a true ferroelectric[31]. Previous studies showed that the ferroelectric response of $Al_{1-x}Sc_xN$ is very similar for sputtered and MBE- and MOCVD-grown films[7]. However, despite the lower measurement frequency (2 kHz vs. 100 kHz), the extent of the hysteretic currents is much higher for the 5-nm-thin Al(Ga)N layer compared to the 100-nm-thin AlN. The associated physically unrealistic high apparent P_r of the 5-nm-thin layer is

Fig. 4 | Ferroelectric response of AlN grown on on GaN. a J–E loop of sputtered 100-nm-thin AlN grown on GaN measured at 40 kHz. **b** J–E loop of 5-nm-thin Al(Ga)N grown by MOCVD on GaN measured at 2 kHz. The overall current response, including typical ferroelectric displacement current peaks (switching, black) and dielectric/leakage currents (non-switching, red), was recorded separately by pre-polarizing the capacitor to the respective polarity. All measurements were performed at room temperature using a voltage signal with a triangular waveform. The current response was averaged over 100 cycles.
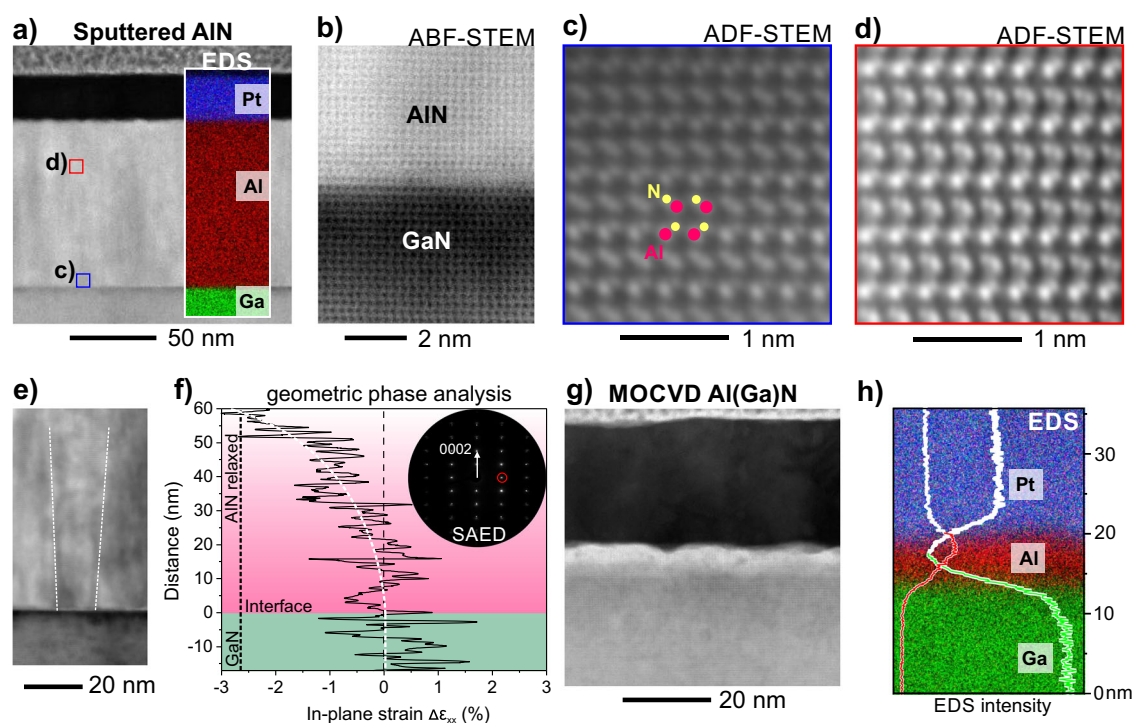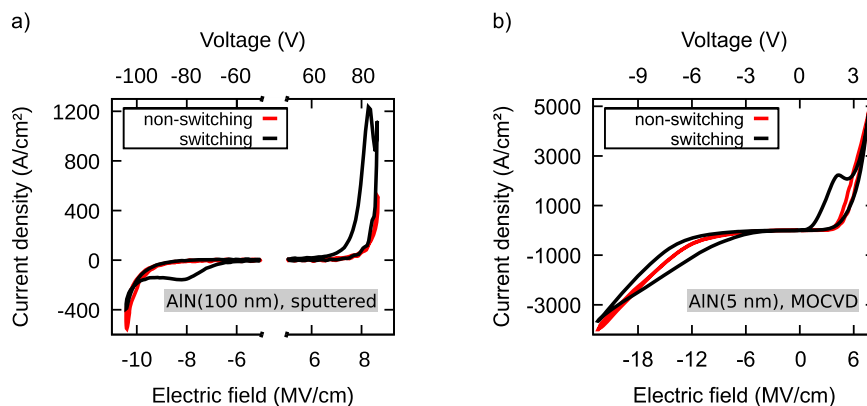
Fig. 5 | Real structure analysis of ferroelectric AlN thin films after ex situ polarization inversion to the N-polar state. a ABF-STEM micrograph and EDS elemental map of the sputtered AlN/GaN heterostructure. **b** HRSTEM micrograph showing the almost atomically smooth interface. **c** HRSTEM micrograph showing N-polar orientation of AlN close to the interface. **d** HRSTEM micrograph showing N-polar orientation of AlN within the bulk of the film. **e** STEM micrograph of the AlN/GaN interface. The dashed lines indicate a coherently aligned columnar area used for strain calculations. **f** Change of the in-plane lattice strain ($\Delta\varepsilon_{xx}$) with respect to the GaN template calculated from the columnar region. The AlN lattice shows tensile strain at the interface and gradual strain relaxation across 60 nm. The dashed line is added for illustration purposes. **g** STEM micrograph of a 5 nm Al(Ga)N/GaN heterostructure grown by MOCVD. **h** EDS analysis of Al-K and Ga-K peak intensities across the heterostructure interface. Note, the white lines display the increase of Ga-K and Al-K background intensity by the increasing contribution of the Pt-M peak.

consistent with prior studies on thickness scaling of $Al_{1-x}Sc_xN$, in which the increase of the apparent P_r was related to thickness-dependent dynamic leakage current contributions[30]. Furthermore, E_c extracted from the positive branch of the 5-nm-thin Al(Ga)N film amounts to 4.3 MV/cm (2.2 V), which is almost half as large as for 100-nm-thin AlN. This is another key feature that separates wurtzite from more classical oxide ferroelectrics, for which E_c typically increases with decreasing film thickness. The reduction in switching barrier height is likely related to several intrinsic effects, next to the presence of a finite depolarization field, i.e., the presence of Ga in the AlN matrix increasing local lattice distortions similar to Sc, epitaxial tensile strain (i.e., fully strained to the GaN), as well as interface roughness examined in the "Atomic-scale investigations" section[30].

Atomic-scale investigations

The nanostructure of the AlN/GaN ferroelectric thin film heterostructure was examined by aberration-corrected scanning transmission electron microscopy (HRSTEM) with down to atomic resolution. The results of the STEM analysis of the AlN(100 nm)/GaN sputtered heterostructure and the Al(Ga)N(5 nm)/GaN MOCVD-grown heterostructure are summarized in Fig. 5a–h. Figure 5a displays an overview of the epitaxial AlN(100 nm)/GaN heterostructure. The AlN/GaN interface appears atomically sharp, but the lower structural coherence of the AlN layer to the template results in diffuse ABF-contrast (cf. Fig. 5b). While the ABF mode (angular range, e.g., 10–20 mrad) is sensitive to image elements with a lower atomic mass (Z), the intensity in the high-angle annular dark field (HAADF, e.g., angular range 80–220 mrad) mode is mostly related to Z^2, which can complicate imaging

of light atoms such as nitrogen. However, the influence of diffraction contrast in the ABF mode can complicate the analysis of light atom positions in regions with lower crystalline coherence, e.g., the strained AlN and Al(Ga)N layers examined in this study. Therefore, the polarity of the AlN film after ferroelectric switching from M- to N-polarity was investigated using the annular dark field (ADF) detector collecting electrons scattered under a medium angular range (e.g., 14–63 mrad). The recorded ADF signal is less influenced by diffracted electrons, and the ability to detect the nitrogen atomic positions is enhanced. The respective HRSTEM micrographs recorded at regions close to the GaN interface and within the film bulk clearly show N-polar unit cells, which confirms the genuine polarization inversion presented in Fig. 5c and d. Thus, in contrast to ferroelectric $Al_{0.85}Sc_{0.15}N$ grown by MOCVD[7], no continuously pinned interfacial region with M-polarity is present in AlN grown by sputter epitaxy on GaN.

As discussed in the "Ferroelectric properties" section, ferroelectric switching in AlN is assumed to be enabled by in-plane tensile strain imposed by the epitaxy to the GaN interface. Figure 5e and f presents the distribution of the in-plane strain component within a 15-nm-wide columnar grain. The local change in strain (1 nm spatial resolution) was calculated by geometric phase analysis (GPA) with respect to the GaN reference lattice[37]. The extracted strain profile indicates the presence of in-plane tensile strain at the GaN interface, consistent with the RSM presented in Fig. 2a. The interfacial tensile strain is evident to relax across a range of about 60 nm, which is comparable to compressively strained $Al_{0.72}Sc_{0.28}N$ films sputter-deposited on GaN[19]. The larger oscillations within the strain profile originate from averaging over local areas with changing structural coherence. The presence of interfacial tensile strain within the basal plane contributes to reducing the switching barrier in the AlN layer[23,24]. However, large-scale strain analysis via the evaluation of nanobeam electron diffraction patterns, e.g., by performing 4D-STEM, is necessary to transfer the strain information from a single column to the whole film.

The discussion of the nanostructure and chemical properties of a 5 nm Al(Ga)N barrier layer grown onto GaN by the MOCVD method is presented in Fig. 5g and h. The ABF-STEM micrograph shows the Pt/Al(Ga)N/GaN heterostructure, where the presence of a ~5-nm-thin layer is evidenced by the Z-contrast variations. The interfacial layer roughness originates from the ex situ growth onto the GaN template, which shows less crystal quality than for layers deposited in situ onto a MOCVD re-grown GaN layer. Hence, the growth of individual grains within the Al(Ga)N layer was observed, which lacks the high structural coherence to the template usually observed for MOCVD-grown layers[9]. Due to the high growth temperatures, MOCVD-grown AlN/GaN heterostructures usually show interdiffusion at the interface, resulting in graded Al(Ga)N layers[36]. The chemical analysis by EDS shows the integrated spectral signal intensity distributions of the Al-K and Ga-K peaks across the heterostructure. A graded Al(Ga)N layer with decreasing Ga concentration toward the Pt electrode and Al interdiffusion into the GaN template is observed, see Fig. 5h. The as-grown polarity of the Al(Ga)N layer was confirmed by HRSTEM to be M-polar.

To summarize, STEM confirms the presence of strained regions in sputtered films that go far beyond the critical thickness obtained by, e.g., MOCVD - an aspect that facilitates switching and the absence of cracks also in comparably thick AlN layers. For 5-nm-thin AlN layers deposited by MOCVD on GaN, the expected layer thickness and interdiffusion of GaN were observed. More surprisingly, the rough nature of the AlN film did not prevent ferroelectric switching, thereby raising the prospect that such topography could also be advantageous to initialize switching by locally enhancing the electric field distribution, e.g., creating nucleation sites - an aspect that should be further investigated in future studies.

Conclusion

Overall, a high structural quality and coherence of $Al_{1-x}Sc_xN$ ($0 < x < 0.28$) grown on GaN by sputter epitaxy is revealed. Epitaxial in-plane tensile ($x \leq 0.11$) and compressive ($x \geq 0.18$) strain is identified, affecting the x-dependent ferroelectric properties. Lattice-matching is expected close to $x = 0.11$, for which almost pseudomorphic growth was evidenced. At nearly lattice-matched conditions ($x = 0.08$), exclusive as-grown M-polarity and an exceptionally low out-of-plane mosaicity (258 arcsec) comparable to ferroelectric MOCVD- and MBE-grown $Al_{1-x}Sc_xN$ is revealed. This demonstrates that sputter epitaxy might emerge as a suitable high-throughput deposition method for the growth of all-epitaxial ferroelectric III-N heterostructures containing Scandium.

Ferroelectricity in $Al_{1-x}Sc_xN$/GaN is revealed for the whole x series. Epitaxial in-plane tensile strain improves the coercive field to breakdown field ratio of AlN/GaN, enabling ferroelectricity in the typically non-ferroelectric binary AlN grown by both sputtering and MOCVD. The coercive field ranges from 4.2 MV/cm ($x = 0.28$) up to 8.8 MV/cm (AlN, 100 nm) at a measurement frequency of 40 kHz. Epitaxial strain deforms the crystal lattice, resulting in an almost x-independent $2P_r$ of ≈ 300 μC/cm^2 for $0.06 < x < 0.28$. For 100-nm-thin AlN, a $2P_r$ of 150 μC/cm^2 is evidenced. Ferroelectricity was also revealed in 5-nm-thin AlN grown on GaN by MOCVD. The comparably low E_c (4.2 MV/cm) of the 5-nm-thin AlN, allowing for ferroelectric switching at 2.2 V (2 kHz), is at least partly attributed to the pseudomorphic growth, i.e., the full volume is in-plane tensile-strained. This is also expected to allow for ferroelectric switching of the full AlN volume, resulting in increased $2P_r$ values compared to the partly lattice-relaxed sputtered 100-nm-thin AlN.

These results highlight the availability of two scalable deposition methods for wurtzite ferroelectrics, which feature a so far unmatched combination of high-throughput and technological compatibility; the growth of Sc-free, ferroelectric AlN/GaN by the commercially well-established III-N growth method MOCVD, as well as lattice-matched ($0.08 < x < 0.11$) ferroelectric $Al_{1-x}Sc_xN$ grown on GaN by sputter epitaxy, featuring a MOCVD-like mosaicity. Both approaches enrich the III-N technology platform and are envisioned to advance the merging of ferroelectric and III-N device functionality.

Methods

The sputtered $Al_{1-x}Sc_xN$ layers were deposited onto commercially available n-type Si-doped GaN/Sapphire templates. Prior to the deposition, the templates were cleaned with aceton and subsequently isopropanol in an ultrasonic bath, followed by rinsing with deionized (DI)-water. Sputter epitaxy was performed in an Oerlikon MSQ 200 multisource system. The Sc content was adjusted by varying the power ratio applied to the 4-inch Sc and Al target operated in pulsed DC co-sputtering mode, while the total power was kept constant at 1000 W. The AlN layer was grown using pulsed DC-sputtering by applying 1000 W only to the Al target. All $Al_{1-x}Sc_xN$ were grown under pure N_2 atmosphere at 450 °C. Details about the process can be found elsewhere[19,31].

A 5-nm-thick AlN layer was deposited on an n-type Si-doped GaN/Sapphire template by MOCVD with a commercial close-coupled showerhead system. The Al precursor was trimethylaluminum (TMAl), the N precursor NH_3, and the carrier gas hydrogen. The growth temperature was 1100 °C and the reactor pressure 40 mbar.

The $Al_{1-x}Sc_xN$ as well as the MOCVD-grown AlN layers were capped ex situ (after vacuum break) with 30-nm-thin Pt using DC-sputtering under Kr atmosphere at 400 W. Circular electrodes were structured using lithography and ion beam etching (IBE, Oxford Instruments Ionfab 300). The dry-etching was stopped right after reaching the $Al_{1-x}Sc_xN$ surface, which was monitored using a secondary-ion mass spectrometer (SIMS).

The topography and the absence of abnormally oriented grains (AOGs) of the sputtered $Al_{1-x}Sc_xN$ thin films were analyzed by performing scanning electron microscopy (SEM) using a Zeiss Gemini Ultra 55 microscope, see Supplementary Fig. 6. The chemical composition was determined by energy-dispersive X-ray spectroscopy (SEM-EDS, Oxford x-act) operated at 13 kV. The samples were tilted toward the EDS detector and partly covered with copper tape to prevent charging.

XRD measurements were performed using a Rigaku SmartLab diffractometer (9 kW, CuKα = 1.5406 Å, Ge (220) 2-bounce monochromator, Hypix-3000 detector). The out-of-plane lattice parameters were extracted from symmetric scans of the 0002 reflection. The in-plane lattice parameters

were extracted from the asymmetric $10\bar{1}5$ reflection, and the in-plane mosaicity was extracted from skew-symmetric ϕ-scans of the $Al_{1-x}Sc_xN$ $(10\bar{1}2)$ reflection. The high-resolution reciprocal space maps were recorded with a 0.5° Parallel Slit Analyzer on the detector side.

The ferroelectric measurements were performed using an AixACCT TF 3000 analyzer. The drive voltage was applied to the top electrode. The diameter of the measured circular capacitors ranged from 10 μm to 50 μm. A voltage signal with a triangular waveform was used in all measurements. The PUND sequence was applied to separate ferroelectric displacement currents from static leakage.

For nanoscale structure characterization by scanning transmission electron microscopy (STEM), the sputtered AlN/GaN and MOCVD-grown Al(Ga)N/GaN heterostructures were prepared in cross-sectional geometry by the focused ion beam (FIB) method from ferroelectric switched capacitors. The investigations were performed with a JEOL "NEOARM" / JEM-ARM200F instrument with aberration-correction of the electron probe (CEOS ASCOR) operating at 200 kV, allowing for direct inspection of the unit cell polarity. High-resolution (HRSTEM) analysis was performed using annular bright field (ABF) and annular dark field (ADF) detectors. Chemical analysis was performed by energy-dispersive X-ray spectroscopy (EDS) using a dual detector system with 100 mm² active area each (JEOL). The in-plane strain component of the epitaxial heterostructure was accessed by geometric phase analysis (GPA) calculation after non-rigid registration of a STEM image series[37,38].

Data availability
All relevant data are available from the corresponding author (Georg Schönweger, gmsc@tf.uni-kiel.de) upon reasonable request. The source data of the numerical results are available as Supplementary Data.

References
1. Schönweger, G. et al. Ultrathin $Al_{1-x}Sc_xN$ for low-voltage-driven ferroelectric-based devices. *phys. status solidi RRL* **17**, 2200312 (2022).
2. Guido, R. et al. Thermal stability of the ferroelectric properties in 100 nm-thick $Al_{0.72}Sc_{0.28}N$. *ACS Appl. Mater. Interfaces* **15**, 7030–7043 (2023).
3. Zhu, W. et al. Exceptional high temperature retention in $Al_{0.93}B_{0.07}N$ films. *Appl. Phys. Lett.* **122**, 242902 (2023).
4. Wang, D. et al. An epitaxial ferroelectric ScAlN/GaN heterostructure memory. *Adv. Electron. Mat.* **8**, 2200005 (2022).
5. Tang, Z., Esteves, G. & Olsson, R. H. Sub-quarter micrometer periodically poled $Al_{0.68}Sc_{0.32}N$ for ultra-wideband photonics and acoustic devices. *J. Appl. Phys.* **134**, 114101 (2023).
6. Lu, H. et al. Domain dynamics and resistive switching in ferroelectric $Al_{1-x}Sc_xN$ thin film capacitors. *Adv. Funct. Mater.* **34**, 2315169 (2024).
7. Wolff, N. et al. Demonstration and STEM analysis of ferroelectric switching in MOCVD-grown single crystalline $Al_{0.85}Sc_{0.15}N$. *Adv. Phys. Res.* **3**, 2300113 (2024).
8. Leone, S. et al. Metal-organic chemical vapor deposition of aluminum scandium nitride. *phys. status solidi RRL* **14**, 1900535 (2019).
9. Streicher, I. et al. Understanding interfaces in AlScN/GaN heterostructures. *Adv. Funct. Mater.* **34**, 2403027 (2024).
10. Zhu, W. et al. Strongly temperature dependent ferroelectric switching in AlN, $Al_{1-x}Sc_xN$, and $Al_{1-x}B_xN$ thin films. *Appl. Phys. Lett.* **119**, 062901 (2021).
11. Hasegawa, K., Shimizu, T., Ohsawa, T., Sakaguchi, I. & Ohashi, N. Full polarization reversal at room temperature in unsubstituted AlN. *Appl. Phys. Lett.* **123**, 192903 (2023).
12. Skidmore, C. H. et al. Proximity ferroelectricity in wurtzite heterostructures. *Nature* **637**, 574–579 (2025).
13. Yang, J. Y. et al. Pulsed e-/d-mode switchable GaN HEMTs with a ferroelectric AlScN gate dielectric. *IEEE Electron Device Lett.* **44**, 1 (2023).
14. Casamento, J. et al. FerroHEMTs: high-current and high-speed all-epitaxial AlScN/GaN ferroelectric transistors. In *2022 International Electron Devices Meeting (IEDM)* (IEEE, 2022).
15. Kumar, R., Gopakumar, G., Abdin, Z. U., Manfra, M. J. & Malis, O. Pinpointing lattice-matched conditions for wurtzite $Sc_xAl_{1-x}N$/GaN heterostructures with x-ray reciprocal space analysis. *Appl. Phys. Lett.* **125**, 052103 (2024).
16. Maeda, T., Wakamoto, Y., Kaneki, S., Fujikura, H. & Kobayashi, A. Structural and optical properties of epitaxial scxal1-xn coherently grown on GaN bulk substrates by sputtering method. *Appli. Phys. Lett.* **125**, 022103 (2024).
17. van Deurzen, L., Nguyen, T.-S., Casamento, J., Xing, H. G. & Jena, D. Epitaxial lattice-matched AlScN/GaN distributed Bragg reflectors. *Appl. Phys. Lett.* **123**, 241104 (2023).
18. Dinh, D. V., Lähnemann, J., Geelhaar, L. & Brandt, O. Lattice parameters of scxal1-xn layers grown on GaN (0001) by plasma-assisted molecular beam epitaxy. *Appl. Phys. Lett.* **122**, 152103 (2023).
19. Schönweger, G. et al. From fully strained to relaxed: epitaxial ferroelectric $Al_{1-x}Sc_xN$ for III-N technology. *Adv. Funct. Mater.* **32**, 2109632 (2022).
20. Yasuoka, S. et al. Effects of deposition conditions on the ferroelectric properties of $(Al_{1-x}Sc_x)N$ thin films. *J. Appl. Phys.* **128**, 114103 (2020).
21. Dreyer, C. E., Janotti, A., de Walle, C. G. V. & Vanderbilt, D. Correct implementation of polarization constants in wurtzite materials and impact on III-nitrides. *Phys. Rev. X* **6**, 021038 (2016).
22. Zhang, S., Fu, W. Y., Holec, D., Humphreys, C. J. & Moram, M. A. Elastic constants and critical thicknesses of ScGaN and ScAlN. *J. Appl. Phys.* **114**, 243516 (2013).
23. Akiyama, T., Miyamoto, T. & Kawamura, T. Effects of Sc composition and lattice constraint on polarization switching of $Sc_xAl_{1-x}N$ alloys: a first-principles study. *phys. status solidi b*, 2400647. https://doi.org/10.1002/pssb.202400647 (2025).
24. Deng, B., Shi, J. & Shi, Y. Molecular dynamics simulations on ferroelectricity of AlN thin films. *J. Am. Ceram. Soc.* https://onlinelibrary.wiley.com/doi/abs/10.1111/jace.20063 (2024).
25. Yasuoka, S. et al. Probing of polarization reversal in ferroelectric (Al,Sc)N films using single- and tri-layered structures with different Sc/(Al+Sc) ratio. *Adv. Mater. Interfaces* **12**, 2400627 (2025).
26. Gremmel, M. & Fichtner, S. The interplay between imprint, wake-up, and domains in ferroelectric $Al_{0.70}Sc_{0.30}N$. *J. Appl. Phys.* **135** (2024).
27. Zhu, W. et al. Wake-up in Al1-xBxN ferroelectric films. *Adv. Electron. Mater.* **8**, 2100931 (2021).
28. Yazawa, K. et al. Anomalously abrupt switching of wurtzite-structured ferroelectrics: simultaneous non-linear nucleation and growth model. *Mater. Horizons* **10**, 2936–2944 (2023).
29. Wolff, N. et al. Electric field-induced domain structures in ferroelectric AlScN thin films. *J. Appl. Phys.* **137**, 084101 (2025).
30. Schönweger, G. et al. In-grain ferroelectric switching in sub-5 nm thin $Al_{0.74}Sc_{0.26}N$ films at 1 v. *Adv. Sci.* **10** (2023).
31. Fichtner, S., Wolff, N., Lofink, F., Kienle, L. & Wagner, B. AlScN: a III-v semiconductor based ferroelectric. *J. Appl. Phys.* **125**, 114103 (2019).
32. Yazawa, K., Drury, D., Zakutayev, A. & Brennecka, G. L. Reduced coercive field in epitaxial thin film of ferroelectric wurtzite $Al_{0.7}Sc_{0.3}N$. *Appl. Phys. Lett.* **118**, 162903 (2021).
33. Kanyandekwe, J. et al. Impact of growth conditions on aln/gan heterostructures with in-situ sin capping layer. *J. Cryst. Growth* **515**, 48–52 (2019).
34. Godejohann, B. et al. AlN/GaN hemts grown by MBE and MOCVD: impact of Al distribution. *phys. status solidi b* **254**, 1600715 (2017).
35. Storm, D. et al. Ultrathin-barrier AlN/GaN heterostructures grown by rf plasma-assisted molecular beam epitaxy on freestanding GaN substrates. *J. Cryst. Growth* **380**, 14–17 (2013).

36. Streicher, I. et al. Effect of AlN and AlGaN interlayers on AlScN/GaN heterostructures grown by metal-organic chemical vapor deposition. *Cryst. Growth Des.* **23**, 782–791 (2023).
37. Jones, L. et al. Optimising multi-frame adf-stem for high-precision atomic-resolution strain mapping. *Ultramicroscopy* **179**, 57–62 (2017).
38. Jones, L. et al. Smart align-a new tool for robust non-rigid registration of scanning microscope data. *Adv. Struct. Chem. Imaging* https://doi.org/10.1186/s40679-015-0008-4 (2015).

Author contributions
S.F. and G.S. conceived and designed the research. G.S. performed the thin film growth via sputtering, the capacitor structuring, and conducted the electrical and SEM/EDX measurements. N.W. conducted the STEM and STEM-EDX study. M.R.I. performed the XRD measurements. I.S. and S.L. performed the MOCVD growth of AlN. S.F. and L.K. supervised this study. G.S., N.W., and S.F. wrote the manuscript. All authors discussed the data and commented on the manuscript.

Competing interests
The authors declare no competing interests.

Additional information
Supplementary information The online version contains supplementary material available at https://doi.org/10.1038/s43246-025-00962-5.

Correspondence and requests for materials should be addressed to Georg Schönweger.

Peer review information *Communications Materials* thanks the anonymous reviewers for their contribution to the peer review of this work. A peer review file is available

Reprints and permissions information is available at http://www.nature.com/reprints

Publisher's note Springer Nature remains neutral with regard to jurisdictional claims in published maps and institutional affiliations.